

# Journal Pre-proof

Advances, Opportunities and Challenges of Hydrogen and Oxygen Production from Seawater Electrolysis: An Electrocatalysis Perspective

Elnaz Asghari, Muhammad Imran Abdullah, Faranak Foroughi, Jacob J. Lamb, Bruno G. Pollet

PII: S2451-9103(21)00193-9

DOI: <https://doi.org/10.1016/j.coelec.2021.100879>

Reference: COELEC 100879

To appear in: *Current Opinion in Electrochemistry*

Received Date: 9 June 2021

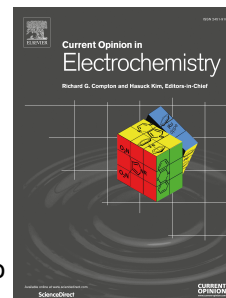
Revised Date: 20 October 2021

Accepted Date: 1 November 2021

Please cite this article as: Asghari E, Abdullah MI, Foroughi F, Lamb JJ, Pollet BG, Advances, Opportunities and Challenges of Hydrogen and Oxygen Production from Seawater Electrolysis: An Electrocatalysis Perspective *Current Opinion in Electrochemistry*, <https://doi.org/10.1016/j.coelec.2021.100879>.

This is a PDF file of an article that has undergone enhancements after acceptance, such as the addition of a cover page and metadata, and formatting for readability, but it is not yet the definitive version of record. This version will undergo additional copyediting, typesetting and review before it is published in its final form, but we are providing this version to give early visibility of the article. Please note that, during the production process, errors may be discovered which could affect the content, and all legal disclaimers that apply to the journal pertain.

© 2021 Elsevier B.V. All rights reserved.



1           **Advances, Opportunities and Challenges of Hydrogen and**  
2                   **Oxygen Production from Seawater Electrolysis:**  
3                           **An Electrocatalysis Perspective**

4           Elnaz Asghari<sup>1\*</sup>, Muhammad Imran Abdullah<sup>2</sup>, Faranak Foroughi<sup>3</sup>, Jacob J. Lamb<sup>4</sup>,  
5   Bruno G. Pollet<sup>3,5</sup>

6  
7           <sup>1</sup>*Electrochemistry Research Laboratory, Department of Physical Chemistry, Faculty of*  
8   *Chemistry, University of Tabriz, Tabriz, Iran*

9  
10          <sup>2</sup>*CAS Key Laboratory of Soft Matter Chemistry, Hefei National Laboratory for Physical*  
11          *Sciences at the Microscale, University of Science and Technology of China, Hefei, Anhui*  
12   *230026, China*

13  
14          <sup>3</sup>*Hydrogen Energy and Sonochemistry Research Group, Department of Energy and Process*  
15          *Engineering, Faculty of Engineering, Norwegian University of Science and Technology*  
16   *(NTNU), NO-7491 Trondheim, Norway*

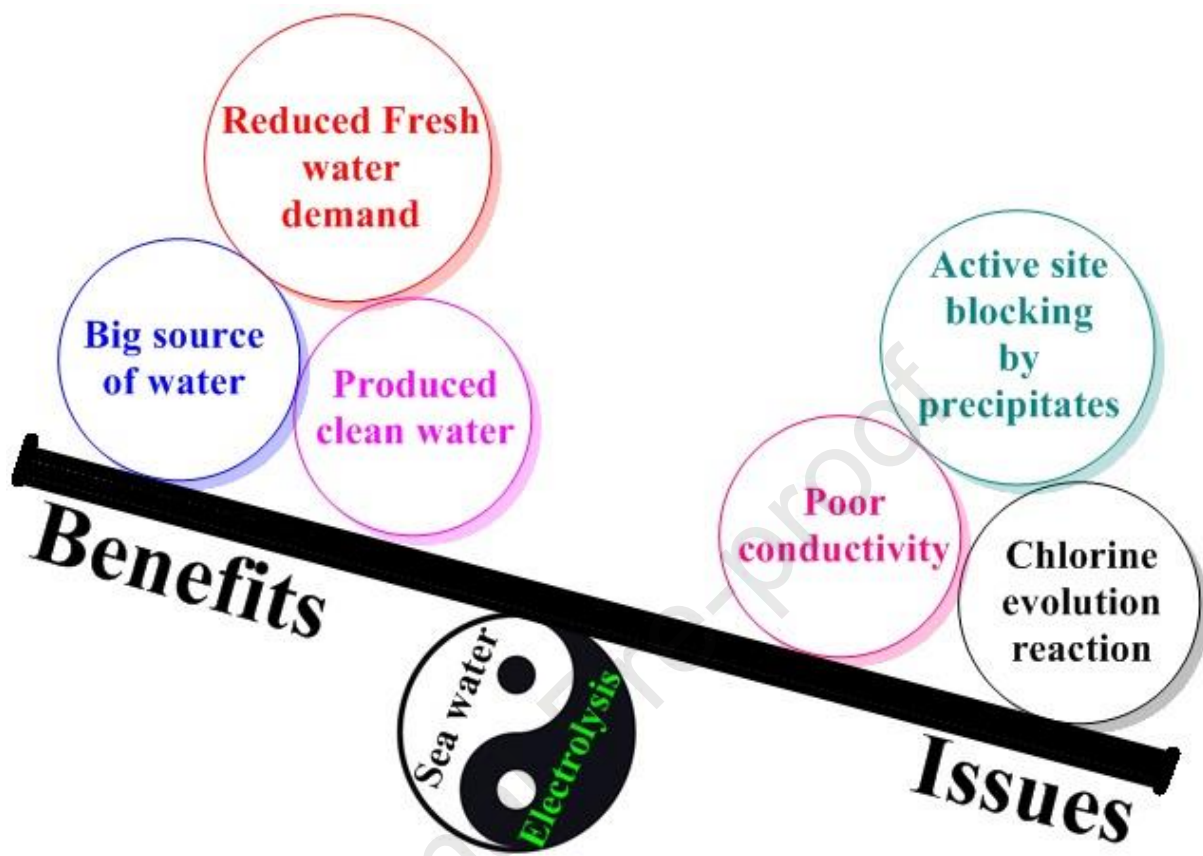
17  
18          <sup>4</sup>*ENERSENSE, Department of Energy and Process Engineering, Faculty of Engineering,*  
19          *Norwegian University of Science and Technology (NTNU), NO-7491 Trondheim, Norway*

20  
21          <sup>5</sup>*GreenH<sub>2</sub>Lab, Pollet Research Group, Hydrogen Research Institute (HRI), Université du*  
22          *Québec à Trois-Rivières (UQTR), 3351 Boulevard des Forges, Trois-Rivières, Québec G9A*  
23   *5H7, Canada*

24  
25          \*Corresponding author: Elnaz Asghari (elnazasghari@yahoo.com and e.asghari@tabrizu.ac.ir)

26 Graphical abstract

27



28

29

30

31 **Abstract**

32         With increasing energy consumption and greenhouse gas emissions, the importance of  
33 developing renewable energy sources to replace fossil fuels has become a vital global task.  
34 Hydrogen produced via water electrolysis powered by renewable energy systems at a large  
35 scale is an essential measure to reduce greenhouse gas and particulate emissions. Electrolysers  
36 use a substantial amount of water (mainly freshwater) to produce hydrogen and oxygen at the  
37 cathode, and anode, respectively. However, seawater is preferred because it is the most  
38 abundant water resource. Although many R&D efforts on seawater electrolysis have been  
39 carried out since the 1970s, the barriers are the undesired chlorine gas evolution reaction at the  
40 anode, and corrosion induced by chloride ions. Unlike the available data for electrocatalyst  
41 materials based upon platinum group metals in pure solutions, limited data is available for  
42 electrocatalysts in seawater. Therefore, there is an urgent need to develop new electrocatalysts  
43 for seawater electrolysis.

44  
45  
46 **Keywords:** Seawater electrolysis; Electrocatalyst; Hydrogen evolution reaction (HER);  
47 Oxygen evolution reaction (OER); Chlorine evolution reaction (CER)



## 48 1. Introduction

49 Electrochemical water splitting for hydrogen generation (currently produces around 1%  
50 of global hydrogen) [1] will play a key role in meeting climate change targets. Water  
51 electrolyzers can provide the foundation of a sustainable hydrogen production network coupled  
52 to intermittent renewable energy systems [1]. For example, the European Union (EU) has  
53 pledged to reach 2x40 GW of water electrolyzers by 2030 (40 GW in Europe and 40GW in  
54 EU's neighborhood with export to the EU) corresponding to up to 20million tons of renewable  
55 hydrogen, with the industry expecting a dramatic exponential increase in water electrolyzers  
56 manufacturing. Also, the world's largest seawater hydrogen production plant in Saudi Arabia,  
57 powered by 4 GW of wind and solar energies, will produce 650 tons of green hydrogen daily  
58 [1,2].

59 Depending upon the catalysts, electrolytes, separators, working temperatures, and  
60 pressures, currently there are five technologies for water electrolyzers [1]:

- 61 (i) Alkaline Water Electrolyser (AWE),
- 62 (ii) Proton Exchange Membrane Water Electrolyser (PEMWE),
- 63 (iii) Anion Exchange Membrane Water Electrolyser (AEMWE),
- 64 (iv) Solid Oxide Electrolysis Cell (SOEC) , and
- 65 (v) Protonic Ceramic Electrolysis Cell (PCEC)

66 PEMWE and AWE are being used commercially as the technology is fairly mature. In  
67 the case of AEMWE, it is now seen as the most promising low-temperature electrolyser  
68 technology. For both PEMWE and AEMWE, membrane electrode assemblies (MEA) are used.  
69 MEAs are usually made of either catalyst coated substrates (CCS) or catalyst coated  
70 membranes (CCM) [1].

71 Low-temperature water electrolyser technologies use a large amount of freshwater  
72 supplies to produce H<sub>2</sub> (i.e., ca. 9litres of pure water per 1kg of H<sub>2</sub>; assuming 100% efficiency).

73 40GW of installed electrolyzers in the EU would represent 10million tons of H<sub>2</sub> and 90million  
74 liters of freshwater [1]. Thus, producing hydrogen from seawater seems to be a very attractive  
75 alternative, especially in regions where freshwater is an issue. Globally, the Middle East, South  
76 Africa, the west coast of the Americas, Australia, and the west of China are the main desert  
77 coastal lands of the world appropriate for solar-driven seawater electrolysis [2-6].

78 Freshwater electrolysis results in the hydrogen evolution reaction (HER) and the oxygen  
79 evolution reaction (OER) on the cathode and the anode of the electrolyser, respectively. Due  
80 to the complex chemical and biological composition of seawater, especially high  
81 concentrations of Cl<sup>-</sup> (*ca.* 3.5wt%, 0.5M, pH~8), the chlorine evolution reaction (CER)  
82 competes with the OER on the anode [7]. Hence, selective, stable, and cost-effective catalysts  
83 are required for seawater electrolyzers to efficiently drive the HER and the OER only. Table 1  
84 summarizes the standard redox potentials for HER and OER in various pH ranges [5,6]. HER  
85 is generally described in two ways: H<sup>+</sup> reduction in acidic media and water reduction in alkaline  
86 media with traditionally accepted mechanism composed of well-known *Volmer*, *Heyrovsky*,  
87 and *Tafel* steps (the corresponding reactions are presented in Table 1) [1]. The classically  
88 accepted 4-electron mechanism of OER in acidic and alkaline media is also given in Table 1  
89 and Figure 1(a).

90 Herein a short discussion of state-of-the-art precious metal-free catalysts for seawater  
91 electrolysis is presented, focusing on advances and challenges with electrocatalysts.

92

93

94 **Table 1.** The hydrogen evolution, the oxygen evolution and the chlorine evolution reaction mechanisms in water, seawater and brine.

Reaction		Half-Reaction	Standard Redox Potential (V) vs. SHE	Mechanism		
HER (low pH's)		$2\text{H}^+ + 2\text{e}^- \rightarrow \text{H}_2$	$E^\ominus = 0.000 \text{ V, pH } 0$	HER [1,5,6]	$\text{H}^+ + \text{e}^- \rightarrow \text{H}_{\text{ads}}$ $\text{H}_2\text{O} + \text{e}^- \rightarrow \text{H}_{\text{ads}} + \text{OH}^-$	Volmer
HER (neutral pH's)		$2\text{H}_2\text{O} + 2\text{e}^- \rightarrow \text{H}_2 + 2\text{OH}^-$	$E^\ominus = -0.827 \text{ V, pH } 14$		$\text{H}_{\text{ads}} + \text{H}_{\text{ads}} \rightarrow \text{H}_2$	Tafel
HER (high pH's)		$2\text{H}_2\text{O} + 2\text{e}^- \rightarrow \text{H}_2 + 2\text{OH}^-$	$E^\ominus = -0.827 \text{ V, pH } 14$		$\text{H}_{\text{ads}} + \text{H}^+ + \text{e}^- \rightarrow \text{H}_2$ $\text{H}_{\text{ads}} + \text{H}_2\text{O} + \text{e}^- \rightarrow \text{H}_2 + \text{OH}^-$	Heyrovsky
OER		$2\text{H}_2\text{O} \rightarrow \text{O}_2 + 4\text{H}^+ + 4\text{e}^-$	$E^\ominus = +1.229 \text{ V, pH } 0$	OER [1,5,6]	In acidic media : $\text{M} + \text{H}_2\text{O} \rightleftharpoons \text{MOH} + \text{H}^+ + \text{e}$ $\text{MOH} + \text{OH}^- \rightleftharpoons \text{MO} + \text{H}_2\text{O} + \text{e}$ $2\text{MO} \rightleftharpoons 2\text{M} + \text{O}_2$ $\text{MO} + \text{H}_2\text{O} \rightleftharpoons \text{MOOH} + \text{H}^+ + \text{e}$ $\text{MOOH} + \text{H}_2\text{O} \rightleftharpoons \text{M} + \text{O}_2 + 2\text{H}^+ + 2\text{e}$  In alkaline media : $\text{M} + \text{OH}^- \rightleftharpoons \text{MOH} + \text{e}$ $\text{MOH} + \text{OH}^- \rightleftharpoons \text{MO} + \text{H}_2\text{O} + \text{e}$ $2\text{MO} \rightleftharpoons 2\text{M} + \text{O}_2$ $\text{MO} + \text{OH}^- \rightleftharpoons \text{MOOH} + \text{e}$ $\text{MOOH} + \text{OH}^- \rightleftharpoons \text{M} + \text{O}_2 + \text{H}_2\text{O} + \text{e}$	
OER (high pH's)		$2\text{OH}^- \rightarrow \text{O}_2 + \text{H}_2\text{O} + 2\text{e}^-$	$E^\ominus = +0.402 \text{ V, pH } 14$			
Chlorine evolution reaction (CER)		$2\text{Cl}^- \rightarrow \text{Cl}_2 + 2\text{e}^-$	$E^\ominus = +1.358 \text{ V, pH } 0$			
Hypochlorate formation (Electrochlorination)		$\text{Cl}^- + 2\text{OH}^- \rightarrow \text{ClO}^- + \text{H}_2\text{O} + 2\text{e}^-$	$E^\ominus = +0.810 \text{ V, pH } 14$			
Chlor-alkali	Cathode	$2\text{H}_2\text{O} + 2\text{e}^- \rightarrow \text{H}_2 + 2\text{OH}^-$ $\text{H}_2\text{O} + 1/2 \text{O}_2 + 2\text{e}^- \rightarrow 2\text{OH}^-$ (for ODC technology)	$E^\ominus = -0.827 \text{ V, pH } 14$ $E^\ominus = +0.402 \text{ V, pH } 14$			
	Anode	$2\text{Cl}^- \rightarrow \text{Cl}_2 + 2\text{e}^-$	$E^\ominus = +1.358 \text{ V, pH } 0$			

95 M: Metal

96

97

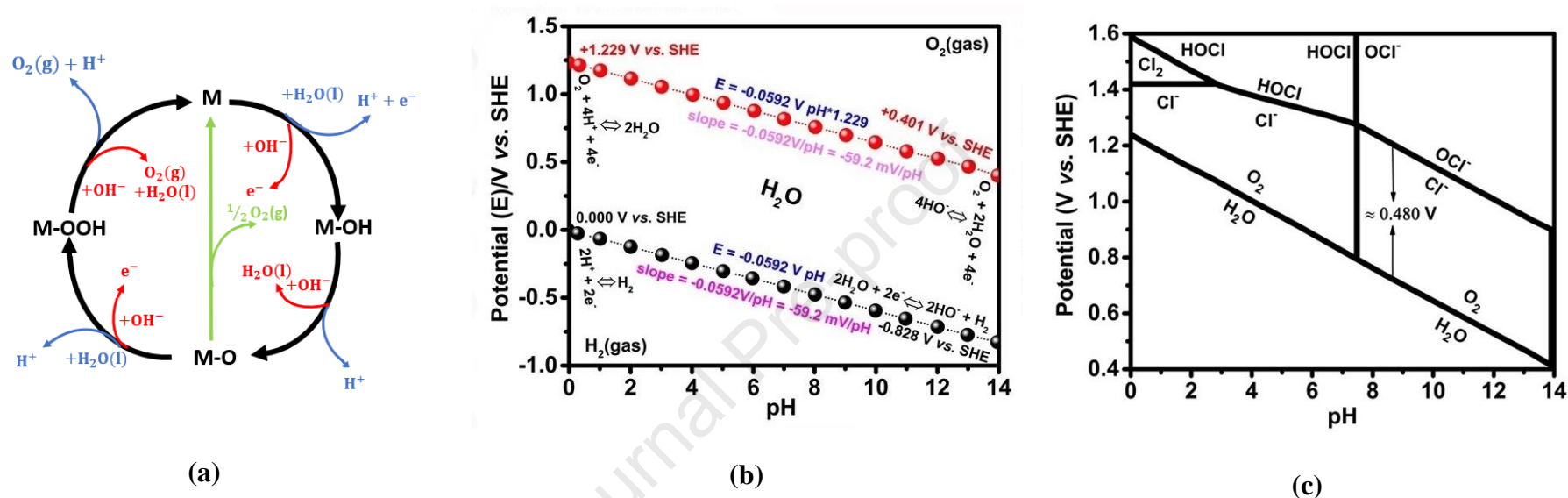


**Figure 1.** (a) The OER mechanism in acid (blue line) and alkaline (red line) solutions. The black line illustrates the OER involving the formation of a peroxide (M–OOH) intermediate, while another possible route for producing oxygen is the direct reaction of two adjacent oxo (M–O) intermediates (green line); representation modified from [6]. (b) The Pourbaix diagram of aqueous electrolyte at 298.15K. (c) The Pourbaix diagram of saline water at 298.15K. Modified from [5,6].

98

## 99 2. Electrochlorination and chlor-alkali processes

100 The electrochlorination and chlor-alkali processes involve electrolysis of seawater and  
101 brine, respectively; the former is often used for water disinfection ( $\text{Cl}_2$ ,  $\text{HOCl}$ , and  $\text{ClO}^-$  are  
102 formed - see Table 1), while the latter producing  $\text{Cl}_2(\text{g})$ ,  $\text{H}_2(\text{g})$ , and  $\text{NaOH}(\text{l})$ . Since the 19<sup>th</sup>  
103 century, four technologies have been developed in the chlor-alkali industry [7,8]:

104 (i) Mercury (Hg) cell: The anodic CER is integrated with sodium amalgam generation  
105 reaction ( $2\text{Hg} + 2\text{Na}^+ + 2\text{e}^- \rightarrow 2\text{NaHg}$ ) on the liquid Hg cathode. Because of the isolated  
106  $\text{Cl}_2$  and NaOH formation, the cell usually generates purer NaOH than later technologies  
107 but with higher energy consumption [7].

108 (ii) Diaphragm cell: A spongy asbestos mat isolates the anode and cathode reactions, and  
109 NaOH is generated in the cathode compartment.

110 (iii) Membrane cell: A polymer ion exchange membrane is used as a separator instead of a  
111 diaphragm with the process similar to the diaphragm cell [7].

112 (iv) Oxygen depolarized cathode (ODC) cells: The formation of hydrogen is prevented by  
113 electrochemical reduction of oxygen to  $\text{OH}^-$  ( $\text{H}_2\text{O} + 1/2\text{O}_2 + 2\text{e}^- \rightarrow 2\text{OH}^-$ ) with ~30%  
114 energy saving. The reaction takes place in the “three-phase zone” of ODC where  $\text{O}_2(\text{g})$ ,  
115 water (liquid), and electrons (from the solid phase) meet [8]

116 Consumable graphite-based anodes are being substituted by the so-called dimensionally  
117 stable anode (DSA) (also called mixed metal oxide (MMO); a platinum group metal, PGM-  
118 based oxide such as  $\text{PtO}_2$ ,  $\text{IrO}_2$  or  $\text{RuO}_2$  coated onto Ti) [7].

119 Figure 1(b) shows the  $E$ - $pH$  (Pourbaix) diagrams of water redox reactions and Figure  
120 1(c) exhibits the Pourbaix diagrams for the seawater redox reactions. The two-electron CER  
121 pathway is kinetically favored over the four-electron OER mechanism. To compensate for this,  
122 the thermodynamic potential difference of the two reactions must be maximized (~480mV at

123 pH >7.5) according to Figure 1(c). As observed in the figure, at low pH the CER, and high pH  
124 the ClO<sup>-</sup> formation compete with the OER. Thus, seawater splitting anodes must be efficient  
125 and sufficiently selective for OER in large-scale applications to avoid the CER [5,6].

### 126 3. Electrocatalysts for HER in seawater

127 Pt is the best platinum group metal (PGM) catalyst for the HER due to the medium  
128 strength of Pt-H bonds and the fast kinetics of HER; but non-PGM catalysts are considered  
129 instead due to the high costs of Pt-based electrodes and stability issues in non-acidic solutions  
130 [9-11]. Even traces of Cl<sup>-</sup> may lead to a significant dissolution of Pt. The loss of electrochemical  
131 active surface area (ECSA) in the presence of 500–2,000ppm Cl<sup>-</sup> and degradation of  
132 electrochemically deposited Pt in the 1-1,000ppm chloride solutions have been reported [12].  
133 Geiger *et al.* [13] also proved that the anodic dissolution occurred via hindering the passive  
134 oxide layers formation in chloride solution; in contrast, the cathodic dissolution was influenced  
135 by the formation of PtCl complexes.

136 Two main strategies to minimize the PGM consumption are to: (i) develop  
137 alloys/composites on supports that help to diminish the precious metals usage, and (ii) design  
138 PGM-free catalysts.

139 Pt-based hollow structures (Pt@mh-3D MXene<sup>1</sup>) with highly porous structures present  
140 large surface areas, enormous adsorption sites, and enhanced diffusion paths; the efficient H-  
141 adsorption, moderate H-binding and rapid water dissociation characteristics also give them  
142 improved performances but lower costs comparable to bulk Pt electrodes [14].

143 Binary/ternary metallic nanocomposites such as NiMo nanocomposites are also proposed  
144 as efficient HER catalysts due to the synergism between Ni and Mo. Generally, Mo atoms  
145 usually are H-adsorption sites and Ni atoms are water dissociation centers [15].

---

<sup>1</sup> MXene: a 2D category of metallic materials with the general formula of M<sub>n+1</sub>X<sub>n</sub>T<sub>x</sub> (n=1-3; M: an early transition metal; X: C or N; T: surface groups like -OH, -O or -F)

146 Binary RuCo/Ti alloy electrodes with Ru as the primary catalytic component and surface  
147 roughness higher than ternary RuCoMo<sub>x</sub>/Ti alloys indicated better HER performances in  
148 filtered seawater. This was due to the effect of surface roughness in enhancing the number of  
149 active HER catalytic sites. Partial oxidation of Ru also resulted in reducing the adsorption  
150 strength on surface sites [16].

151 Transition-metal di-chalcogenides (TMDs) such as MoS<sub>2</sub> have been known for many  
152 decades, but their catalytic activity remained unknown due to their low conductivity. Their  
153 catalytic activity is improved by forming nanostructures, doping metallic atoms like Co and Ni  
154 on edge sites and incorporating 2D carbon materials [15].

155 Intrinsic catalytic activity, porous structure and oxygen vacancies of transition metal  
156 oxides (TMOs) make them more appropriate for HER catalysis [15]. For CoFe<sub>2</sub>O<sub>4</sub>  
157 nanoparticles the physical properties were regulated by tuning their oxygen vacancies as a  
158 function of particle size and worked under a very low cell voltage of 1.47V at 80<sup>o</sup>C in an  
159 alkaline seawater electrolyser [17].

160 Generally, catalysts with adjacent metal oxide (MO<sub>x</sub>) or metal (M) sites weaken the H-  
161 OH bonds since the MO<sub>x</sub> sites tend to adsorb OH<sup>-</sup> ions, while the nearby M sites prefer an H-  
162 bonding. Recently, Mn-based metal organic frameworks (MOFs), with nickel oxide anchored  
163 on nickel foam (NF) (Mn-NiO-Ni/NF), have been introduced as efficient catalysts in seawater.  
164 NF was the source of NiO and the pyrolysis of Mn-MOF yielded a MnO/C composite. The  
165 carbon matrix facilitated the formation of Mn/Ni composites. The electrodes showed onset  
166 potentials lower and current densities higher than commercial Pt/C in seawater. Regardless of  
167 scale deposition at long-term electrolysis, Mn-NiO-Ni/NF showed small activity losses at  
168  $\eta \sim 140\text{mV}$  with  $j \sim 7\text{mA/cm}^2$  for 14h [18].

169 The close contact of the electrocatalyst with substrate and the synergism between  
170 catalytic phases decrease the charge transfer resistances ( $R_{ct}$ ) and improve efficiency and

171 durability. Ni-based TMOs mostly composed of  $\alpha$ -Ni(OH)<sub>2</sub> and Ni sites converted from NF  
172 substrates are some examples. With electron transfer from  $\alpha$ -Ni(OH)<sub>2</sub> sites to the adjacent Ni  
173 sites, slightly negative charges on Ni sites are formed that triggers the proton adsorption; the  
174 positively-charged Ni(OH)<sub>2</sub> sites also weaken the H-OH bonds, promoting water dissociation  
175 that improves the catalyst performance and durability [19].

176 Transition metal phosphides (TMPs) are also considered as one of the most promising  
177 categories of non-PGM HER catalysts, especially in acidic solutions [15]. Despite the high  
178 electrical conductivity, stability, and catalytic performance of TMPs in pure aqueous solutions,  
179 limited data are available in seawater. Recently, porous 3D feather-like NiCoP nanoarrays on  
180 NF (PF-NiCoP/NF) indicated high HER activity in seawater, showing an onset potential of -  
181 287mV with a FE of 96.5%. The NiCo nanoarrays were synthesized on NF via a hydrothermal  
182 method followed by a phosphorization step at 300°C under an N<sub>2</sub> atmosphere. Synergism  
183 between Ni and Co phosphides, 3D network and high porosity of the NiCoP perpendicularly  
184 grown on NF, facilitate the diffusion of produced gases and mass transport of H<sup>+</sup>/H<sub>2</sub>O, increase  
185 the *ECSA* and provide many adsorption sites. The overpotential of PF-NiCoP/NF has been  
186 compared with other NiP-based electrodes in Figure 2(a). As observed, the reduced HER  
187 overpotential on PF-NiCoP/NF electrodes signifies the effect of morphology on electrode  
188 performance. In natural seawater, these structures indicated the HER performance even better  
189 than Pt/C electrodes. Under cathodic overpotential of 290mV, the electrode response remained  
190 unchanged after 20h of electrolysis. Despite this, white scales precipitated on the electrode,  
191 which were entirely removed with dilute acid washing, and the electrode worked again for 12h  
192 without significant degradation [20].

193 Generally, in TMPs, higher electronegativity with high P-content increase the number  
194 of negatively charged sites (for H-adsorption). Elevated P-content can also improve the



195 corrosion resistance and stabilities; however, its further enhancement has adverse effects on  
196 electrocatalytic performance because of the conductivity reduction [15].

197 It was found that doping nitrogen in the carbon shell of CoMoP@C core-shells made  
198 them more appropriate for seawater electrolysis. The N-doped carbon shell protected the  
199 CoMoP core from poisoning and corrosion with no significant current loss in artificial seawater  
200 and just slight decline in real seawater. Gibbs free energy of H-adsorption for N-doped samples  
201 was much lower than un-doped CoMoP@C. The electron-donating tendency of CoMoP,  
202 electron-withdrawing nature of N and high conductivity of C made a facilitated electron  
203 transfer path CoMoP→C→N; carbon shell also acts as an active HER catalytic site due to its  
204 high electron density [21].

205 Nanocomposites of transition metal carbides (TMCs) like WC and W<sub>2</sub>C with high  
206 mechanical robustness and corrosion resistance also improve the stability of the catalysts. For  
207 example, Pt monolayers (MLs) or nanoparticles revealed low adhesion to the commonly used  
208 carbonaceous supports, causing low integrities that were improved significantly using WC and  
209 W<sub>2</sub>C due to the strong binding energies between Pt and WC/W<sub>2</sub>C. Carbon supports with high  
210 porosities but low intrinsic HER catalysis properties show gradual degradation. TMCs provide  
211 better intrinsic catalytic properties, higher stabilities, and strong binding to the upper layer [22].  
212 Bimetallic TMCs of Co<sub>3</sub>Mo<sub>3</sub>C with carbon nanotubes (CNT) on NF (Co<sub>3</sub>Mo<sub>3</sub>C/CNT/NF)  
213 showed a Tafel slope and  $j_0$  of 249mV/dec and 415 $\mu$ A/cm<sup>2</sup>, respectively ( $j_0$  ~13 times larger  
214 than bare NF) due to larger active surface area and higher catalytic activity of Co<sub>3</sub>Mo<sub>3</sub>C/CNT  
215 [9].

216 We have summarized a list of recently studied PGM-free electrocatalysts for HER and OER in  
217 seawater in Table 2.

**Table 2:** A summary of PGM-free electrocatalysts for HER and OER in different electrolytes

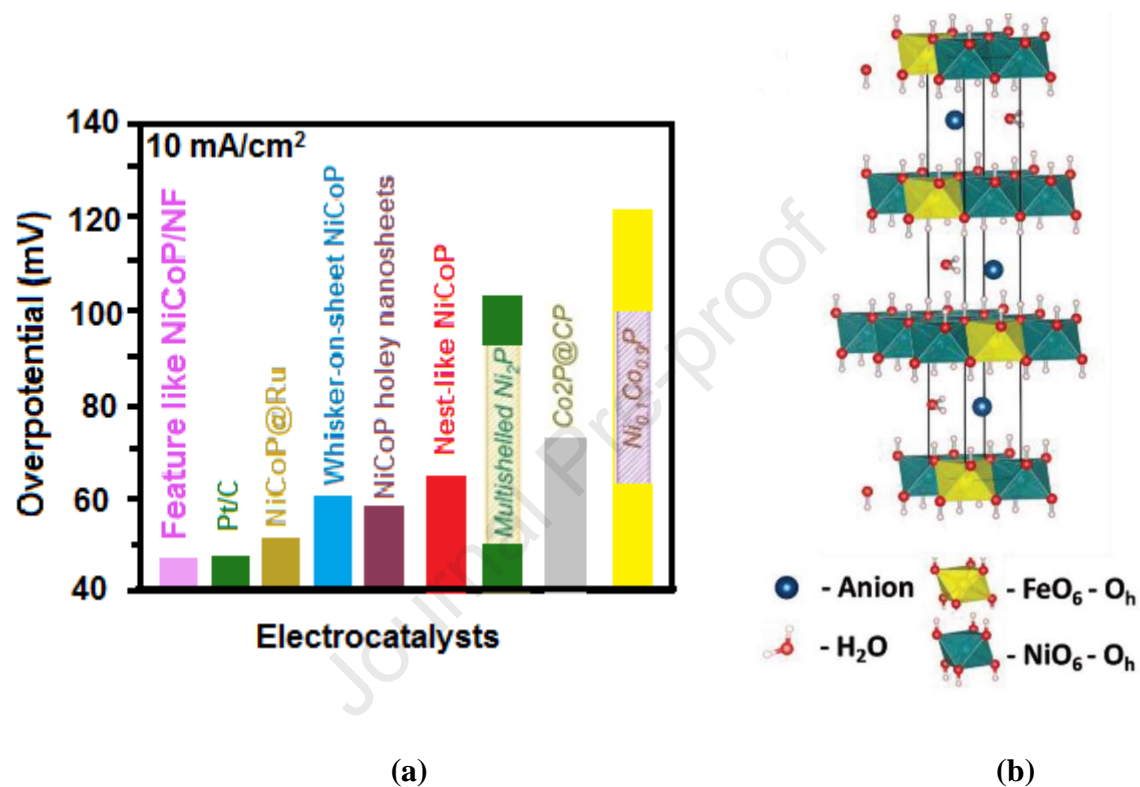
<b>HER</b>					
<b>HER Catalyst</b>	<b>Performance</b>	<b>Electrolyte</b>	<b>Tafel slope (mV/dec)</b>	<b>Highlights</b>	<b>Ref.</b>
Ni <sub>2</sub> P-Fe <sub>2</sub> P	$\eta \sim 41$ mV at 10 mA/cm <sup>2</sup>	1 M KOH 1 M KOH + seawater	86	Bi-functional HER/OER catalyst with almost similar efficiencies in both KOH and KOH + seawater	[23]
Co <sub>3</sub> Mo <sub>3</sub> C/CNT/Ni-F*	$\eta_{\text{onset}} = 42$ mV $j_0 = 0.415$ mA/cm <sup>2</sup>	Seawater	249	Persistent operation over 26 h	[9]
Nanosheets, Mo <sub>5</sub> N <sub>6</sub>	$\eta = 257$ mV at 10 mA/cm <sup>2</sup>	Natural seawater	-	Extremely stable H <sub>2</sub> production for 100 h at an overpotential of 300 mV	[24]
(Ni, Ru, Ir)-G**	-	Real seawater	48	A low overpotential of 0.08 V for 250 cycles; constant current density for 200 h; almost a 100% H <sub>2</sub> production efficiency.	[11]
ReS <sub>2</sub> -T/Td	$j_0 = 54.7$ $\mu$ A/cm <sup>2</sup>	Saline water	69.5	Stable HER performance for over 12 h	[10]
NiCoP@Ni-F	$\eta = 287$ mV at 10 mA/cm <sup>2</sup>	Seawater	54	Increased active surface area and adsorption sites; efficient electron-transfer due to 3D structure	[20]
N-doped CoMoP@C	$\eta_{\text{onset}}$ not as good as Pt/C	Simulated and real seawater	49.73	N-doped carbon shell protected the CoMoP core from poisoning and corrosion	[21]
Binary RuCo and ternary RuCoMo <sub>x</sub> on Ti foils	$\eta_{\text{onset}} = 370$ mV for RuCo	Seawater	>107 (RuCo)	Higher Ru amount and the rougher surface yield higher activity; stable for over 12 h	[16]
<b>OER</b>					
<b>OER Catalyst</b>	<b>Performance</b>	<b>Electrolyte</b>	<b>Tafel slope (mV/dec)</b>	<b>Highlights</b>	<b>Ref.</b>
NiO/FTO*** coated glass	$\eta = 340$ mV at 10 mA/cm <sup>2</sup>	1.0 M KOH 0.5 M NaCl	-	Dimensional stability increased due to the lack of metallic phase,	[25]
Fe-Ni(OH) <sub>2</sub> /Ni <sub>3</sub> S <sub>2</sub>	$\eta = 269$ mV to at 10 mA/cm <sup>2</sup>	Alkaline artificial seawater	46	Heterogeneous lamellar-edged. 27 h work at 100 mA/cm <sup>2</sup>	[26]
Bimetallic oxy-boride (Co-Fe-O-B)	$\eta = 294$ mV at 10 mA/cm <sup>2</sup>	1.0 M KOH + 0.5 M NaCl	52.6	Lowering the charge-transfer resistance. 100% O <sub>2</sub> selectivity	[27]
Ni borates and Co phosphates	-	0.5 M NaCl and seawater	-	CoPi and NiBi selectively generated O <sub>2</sub> suppressing the oxidation of Cl <sup>-</sup> and Br <sup>-</sup>	[28]
Se-NiFe-LDH****	-	Seawater-like electrolyte	26.3	250 h operation with a Se incorporated phase; large SeO <sub>x</sub> <sup>-</sup> ions suppressed the corrosion via Cl <sup>-</sup> repulsion	[29]

NiFeN decorated on NiMoN nanorods on the Ni-F NiMoN@NiFeN	$\eta = 277$ mV for 100 mA/cm <sup>2</sup>	Alkaline seawater	58.6	High conductivity of nanorods; large active surface area; formation of thin amorphous layers → corrosion resistance 3D structure → facilitates the diffusion of reactants and products	[30]
3D bifunctional CoSe (Co <sub>9</sub> Se <sub>8</sub> )	$\eta = 280$ mV at 100 mA/cm <sup>2</sup>	Seawater	40.4	High activity and stability over both HER and OER; stable for 2,000 cycles in 1.0 M KOH	[31]
*CNT: carbon nanotube; Ni-F: Nickel Foam; **G: Graphene; *** FTO: fluorinated titanium oxide; ****LDH: layered double hydroxide					

219

220

221



222

223

224

225

226

**Figure 2:** (a) Comparison of the HER overpotential<sup>2</sup> for different nanostructured electrocatalysts [*reproduced from ref. 20*] (b) Crystal structure of NiFe-LDH with H<sub>2</sub>O and CO<sub>3</sub><sup>2-</sup> ions in the interlayer. The nickel and iron are octahedrally (Oh) surrounded by oxygen atoms

[*reported from ref. 40*]

<sup>2</sup>Overpotential was considered as the potential with respect to the equilibrium potential

#### 4. Electrocatalysts for the OER in seawater

Iridium and ruthenium oxides (such as IrO<sub>2</sub>/Ti) are highly efficient OER catalysts in non-chloride solutions but not selective in seawater [32]. Although,  $\gamma$ -MnO<sub>2</sub> layers on IrO<sub>2</sub> can suppress CER blocking the Cl<sup>-</sup> diffusion to the active catalyst layer [33,34].

Nickel oxide [25], layered double hydroxides (LDHs) [29,35,36], lamellar-edged Fe-Ni(OH)<sub>2</sub>/Ni<sub>3</sub>S<sub>2</sub> nanoarrays [26], oxy-borides (Co-Fe-O-B) [27,29,25,36] and Ni/Co oxidic metallates [28] have been reported as selective OER catalysts for seawater electrolysis.

A corrosion-resistant 3D core-shell of NiFeN with NiMoN nanorods on NF exhibited very high current densities at low cell voltages in alkaline seawater. High conductivity of the inner NiMoN nanorods, large surface area, and 3D structure yielded highly active stable electrodes. The high current densities observed even after normalization to *ECSA* confirmed that their improved catalytic performance was not only due to surface area enhancement but also because of their high conductivity, facilitated charge transfer in the catalyst/electrolyte interface, and robust contact between components [30].

Layered double hydroxides (LDHs) are a family of ionic materials composed of brucite-like layers. Counter ions and solvent molecules may enter in their interlayer spacing. The interlayer spacing in these materials can be engineered by doping various metallic atoms (see the crystal structure of the Ni-Fe LDH in Figure 2(b)). Regardless of their great potential as promising non-PGM OER electrocatalysts in freshwater, few of them have been studied in seawater [29,35-38]. Ni-Fe LDH catalysts with a Ni/Fe ratio of 3.6 were reported for seawater OER catalysis by Dresp *et al.* [39]. Ni-Fe LDH deposited on a Se-covered NiFe foam proved decreased overpotential and Tafel slope and enhanced lifetime (~250h) in artificial seawater due to enhanced conductivity, protective properties of Se against corrosion, and the synergism between different layers [29]. Dresp *et al.* [40] extensively fabricated an AEMWE using the

251 NiFe-LDH and proved their great potential as promising low-cost selective anodes for real  
252 electrolyzers [35,40,41].

253 Heterogeneous bimetallic phosphides of Ni and Fe ( $\text{Ni}_2\text{P}-\text{Fe}_2\text{P}$ ) on NF with high  
254 intrinsic catalytic activity, micro-sheet structure, enhanced active sites, and a hydrophile  
255 surface were also reported as selective OER catalysts in seawater [23].

256 Lamellar-edged Fe-Ni(OH)<sub>2</sub>/Ni<sub>3</sub>S<sub>2</sub>@NF nanoarrays showed decreased overpotentials  
257 and  $R_{\text{ct}}$  values compared with bare Ni<sub>3</sub>S<sub>2</sub>@NF. They also worked with a negligible activity  
258 decay for 27h at 100mA/cm<sup>2</sup>. Fe sites on lamellar edges were responsible for their raised  
259 activity and selectivity. The 2D structure made high exposed area, more active sites, facile  
260 electron/mass transfer and better gas movement; the Ni<sub>3</sub>S<sub>2</sub> was responsible for corrosion  
261 resistance [26].

262 For anodes made from MnO<sub>2</sub>/Mn<sub>2</sub>O<sub>3</sub> composites with Co<sub>3</sub>O<sub>4</sub> nanoparticles the intrinsic  
263 catalytic activity of Co<sub>3</sub>O<sub>4</sub>, high oxygen defect content, and the oxide/oxide heterojunctions  
264 even in real seawater yielded a FE% ~100% showing their selectivity. They were more durable  
265 in simulated seawater because in real seawater, higher ionic strength decreased the number of  
266 available water molecules at the electrode/electrolyte interface [34].

267

## 268 **5. Challenges with seawater electrolysis from an electrocatalytic perspective**

269 Even the most durable electrodes for seawater electrolyzers have not shown significant  
270 durability at high current densities ( $j > 500\text{mA}/\text{cm}^2$ ). Thus, the development of robust catalysts  
271 is crucial for future seawater electrolyzers [15]. Seawater components also affect the membrane  
272 in PEMWE and AEMWE, as well as the electrolyser performance [36].

273

274

275

## 276 **5.1. Chlorine chemistry interference with OER**

277 For the anode, competition between chlorine chemistry and OER is a challenge and the main  
278 strategies to suppress the chlorine evolution reaction (CER) can be summarized as  
279 [5,34,41,42]:

280 (i) Electrolysis at current densities lower than  $1\text{mA}/\text{cm}^2$ :

281 The OER is thermodynamically preferred at  $j < 1\text{mA}/\text{cm}^2$ ; however, it is not practical for  
282 large  $\text{H}_2$  production [33,42].

283 (ii) CER can be inhibited at an elevated pH:

284 Using a Ni-FeLDH anode, Dionigi *et al.* [35] established a selectivity criterion presented  
285 as the dashed area in Figure 3(a), based on the maximum allowed overpotential of OER  
286 as a function of pH. Operation outside the criterion resulted in severe loss of selectivity  
287 and electrode degradation. In comparison, highly alkaline conditions impose high costs  
288 and triggers the scale deposition on the cathode.

289 (iii) Covering the catalyst with a  $\text{Cl}^-$  blocking layer:

290  $\text{MnO}_x$  coatings were shown to repel chloride ions and prevent its adsorption or diffusion.  
291  $\text{MnO}_x$  is not involved in the OER mechanism but instead acts as a barrier against  $\text{Cl}^-$   
292 diffusion, while remaining permeable to water [33,34].

293 (iv) Coating the anode with a cation exchange membrane (CEM) to hinder the adsorption of  
294  $\text{Cl}^-$  can block the  $\text{Cl}^-$  penetration to the electrode/electrolyte interface; however, it might be  
295 practically challenging because of the high costs of CEMs [43].

## 296 **5.2. Recent strategies for increased selectivity of OER electrocatalysts**

297 Dresp *et al.* [41] performed a study for understanding the structural transformations and  
298 details of  $\text{Cl}^-$  ion interactions with different phases in Ni-Fe LDH anodes. Unlike Ni hydroxide  
299 the Ni-Fe LDH has no  $\beta$ -phases and only include  $\alpha\text{-Ni}(\text{OH})_2 \leftrightarrow \gamma\text{-NiOOH}$  transformations.  
300 They used a grazing incidence (GID) cell with *operando* wide-angle X-ray scattering (WAXS)

301 and recorded CV plots in a KOH solution with and without 0.5M NaCl in various pH  
302 conditions. The presence of NaCl improved the catalytic performance of Ni-Fe LDH and based  
303 upon their previous work, it was not due to the chlorine-related oxidation reactions [36,40].  
304 The increase in OER activity was also observed at an elevated pH. Analysis of the interlayer  
305 spacing (Figure 3(b)) revealed that the incorporated Cl<sup>-</sup> ions stabilize the  $\alpha$ -phase, slowing  
306 down the structural  $\alpha \rightarrow \gamma$  transformations. They also proved that raising pH to 14 enhances the  
307 number of the catalytically active  $\gamma$ -NiFe LDH sites and off-sets the negative effects of chloride  
308 ions on their performance [41]. Despite this, several strategies have been proposed to diminish  
309 the requirement for these anodes for highly alkaline conditions. Lu *et al.* [37] optimized the  
310 alkali treatment amount required for the optimal performance of Ni-Fe LDH on carbon cloth  
311 (CC). They found that alkali treatment of the seawater before electrolysis helps to remove Ca<sup>2+</sup>  
312 and Mg<sup>2+</sup> from seawater. Thereafter, no additional alkali is required to have an OER selectivity  
313 of over 94%. With their suggested method, Tafel slopes of 51 and 52mV/dec were obtained in  
314 treated seawater and pure KOH, respectively, confirming similar mechanisms of OER [37].

315 Currently, most seawater electrolyzers work with symmetric electrolytes at a high pH  
316 and current densities lower than 200mA/cm<sup>2</sup>. Future electrolyzers must work with current  
317 densities of at least 1A/cm<sup>2</sup>. Recently, Dresp *et al.* [36] proposed an asymmetric AEMWE with  
318 direct seawater feed in the cathode compartment (pH ~7-8) and circulating 0.5M KOH in the  
319 anode and a CCM configuration (Figure3(c)) The Ni-Fe LDH anode worked better than Ir-  
320 based anodes up to a cell voltage of 4.0V. Regardless of Cl<sup>-</sup> penetration in trace amounts from  
321 the membrane, no chlorine-related oxidation was observed.

322 Dresp *et al.* [40] also reported an AEMWE with alkaline NaCl electrolyte using an  
323 anode based upon highly crystalline Ni-Fe LDH. In the practical large-scale applications, the  
324 cell may expose successive stop/restart cycles; thus, they investigated their model electrolyser  
325 under similar conditions. Founding a recovery effect after stopping/restarting, they verified that

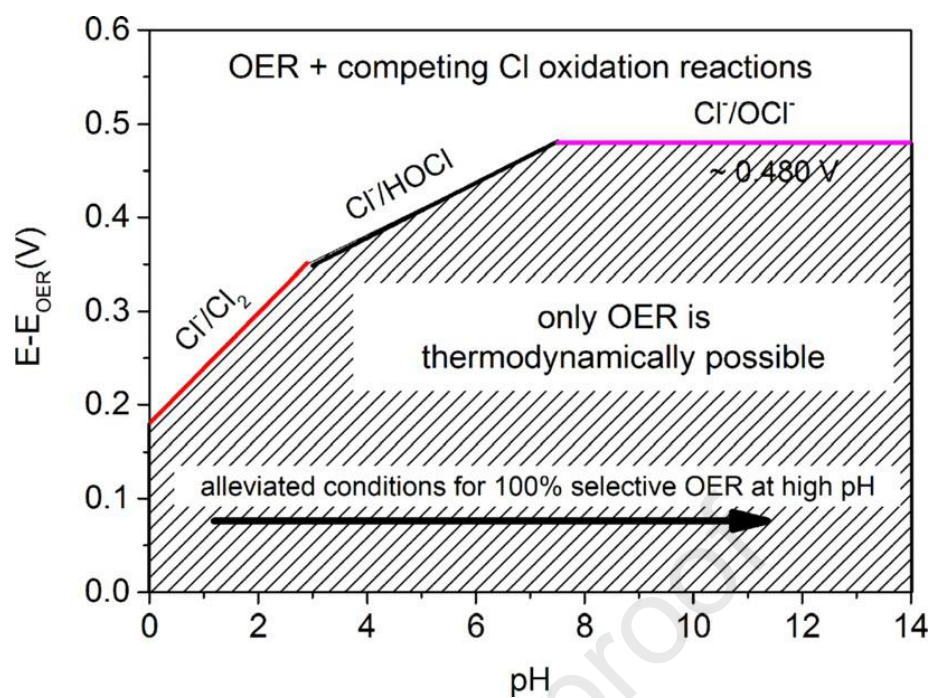


326 a programmed stop/start cycle could improve the cell performance, perhaps due to removing  
327 gas bubbles and partial “chemical resetting” of the metal oxide electrode. The recovery was  
328 less effective with chloride-containing electrolytes. The anode was very selective because a  
329 similar FE% was obtained in NaCl-free and 0.5M NaCl-containing KOH solutions without  
330 traces of chlorine-related species. Long-term stability tests in two protocols (i) 5 days  
331 electrolysis (20h electrolysis at +1.6V and 4h shutdown); and, (ii) 100h continuous electrolysis,  
332 exhibited almost similar results. It opened a way for Ni-Fe LDH based anodes to be introduced  
333 as promising materials for direct seawater electrolysers.

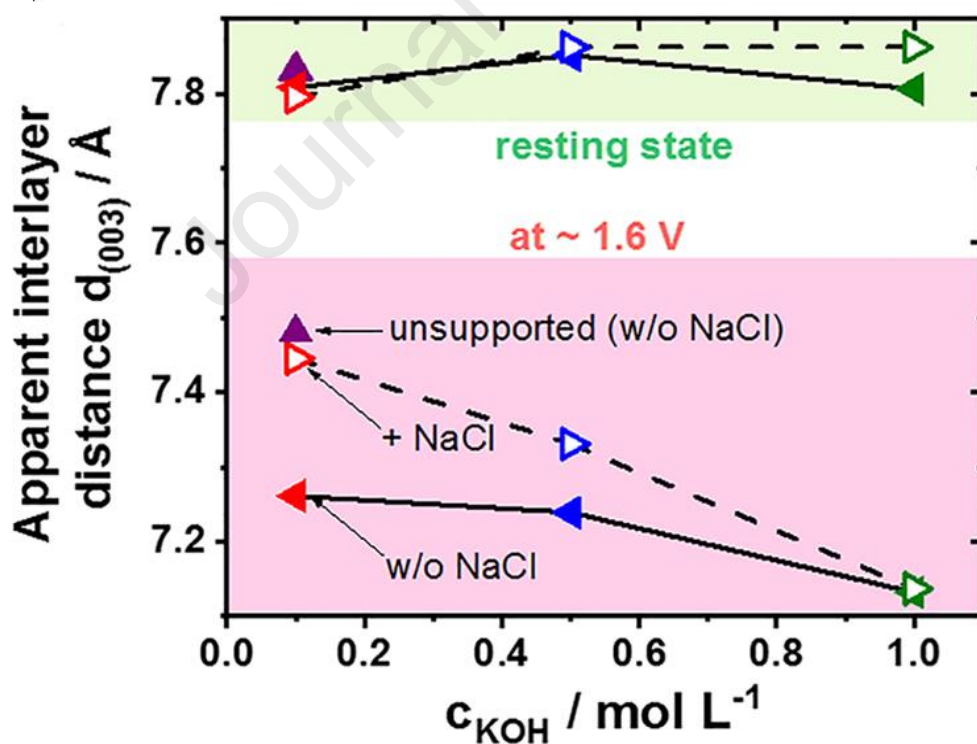
334

335 Amikam *et al.* [42] proposed another innovative water electrolysis system based upon  
336 the salting-out effect for NaCl in NaOH solutions (Figure 3(d)). They removed  $\text{Ca}^{2+}$  and  $\text{Mg}^{2+}$   
337 from seawater feeds using nanofiltration. A settling tank containing 20-40wt% NaOH (~20-  
338 30<sup>0</sup>C) was used for NaCl precipitation. The effluent was injected into an electrolyser with a  
339 Ti/IrO<sub>2</sub>-RuO<sub>2</sub>-TiO<sub>2</sub> anode (temperature > 50<sup>0</sup>C). The high concentrations of OH<sup>-</sup> significantly  
340 suppressed CER. The system was successfully operated at 467mA/cm<sup>2</sup> using NaCl-saturated  
341 NaOH solution for 12days producing ~ 1.2m<sup>3</sup> H<sub>2</sub> and ~150g of precipitated NaCl(s) [42].

342



(a)



(b)

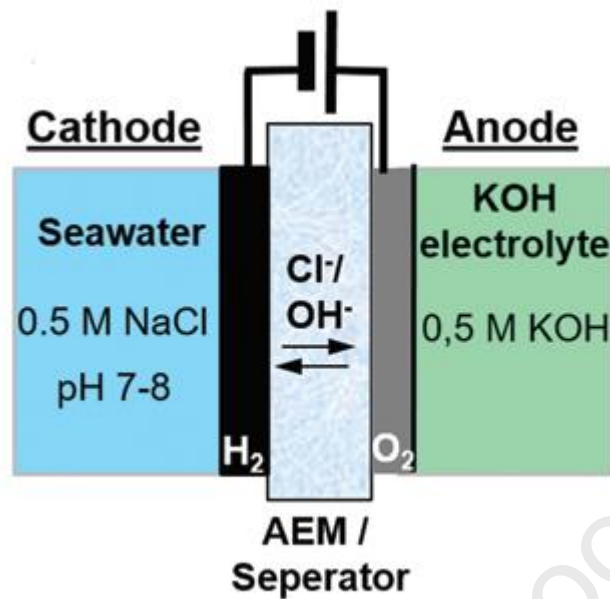
343

344

345

346

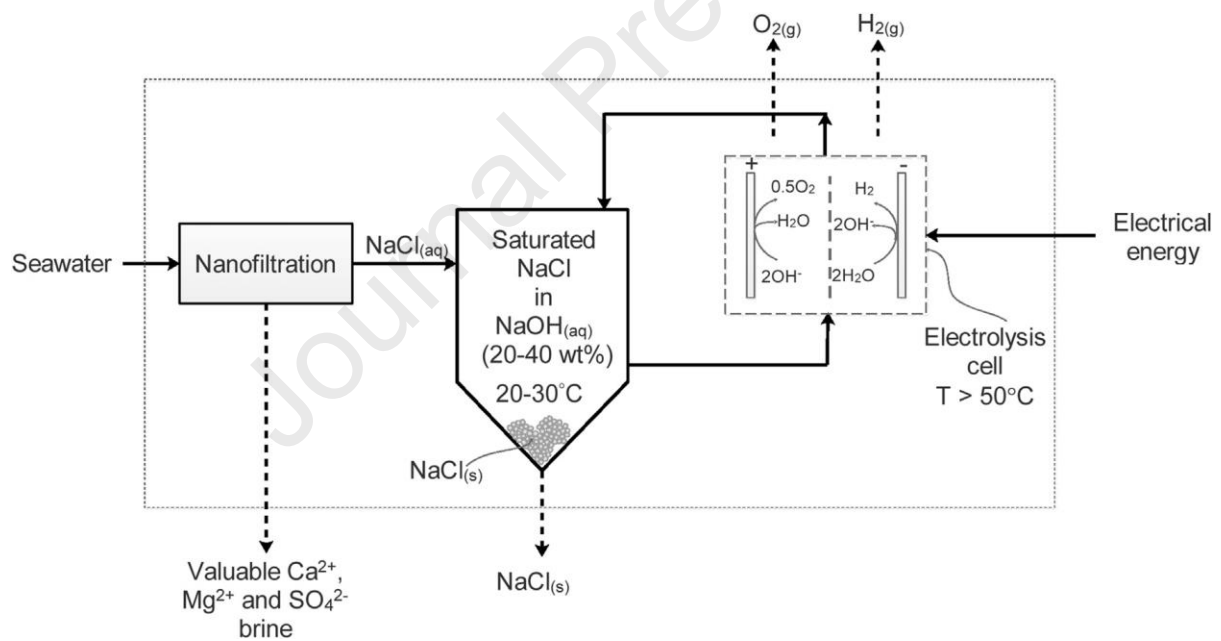
347



348

349

(c)



350

351

352

(d)

353 Figure3: (a) Maximum allowed overpotential of OER electrolyser catalysts to ensure 100%

354 selective water splitting [Reported from ref. 35], (b) overview of the estimated interlayer

355 distance of Ni-Fe LDH with NaCl and KOH concentrations [Reported from ref.41], (c)

356 asymmetric 0.5M NaCl feed at the cathode and 0.5M KOH feed at the anode [Reported from

357 *ref. 36], (d) Process for chlorine-free seawater electrolysis for H<sub>2</sub> (and O<sub>2</sub>) production*  
358 *proposed by Amikam et al. [Reported from ref.42].*

359

### 360 **5.3.Side reactions due to the seawater composition**

361 Based upon a comprehensive table gathered by Dresp *et al.* [5], chloride and bromide  
362 are the most important ions in seawater electrolysis. Although the redox potential of Br<sub>2</sub>/Br<sup>-</sup>  
363 (1.331V *vs.* SHE) is very close to that of Cl<sub>2</sub>/Cl<sup>-</sup> (1.358V *vs.* SHE) due to the low bromide  
364 concentration, its competition with OER is neglected [38,44].

365 Deposition of insoluble compounds such as the Ca(OH)<sub>2</sub> and Mg(OH)<sub>2</sub> on the cathode  
366 with a high pH blocks the active catalytic sites of the electrocatalyst [18,30,42]:



369 Although the adsorption of small amounts of Mg<sup>2+</sup> and Na<sup>+</sup> on the electrodes such as  
370 Co-Fe LDH may enhance the number of strong basic sites and suppress the necessity of  
371 buffering. Cl<sup>-</sup> adsorption may also be beneficial for stabilizing the high oxidation forms of Co  
372 in the catalyst that positively affects their OER activity [45].

373 Corrosion in the aggressive chloride medium also causes electrode degradation. The  
374 corrosive environment and the shear stresses of the fluid flow make the anodes very susceptible  
375 to erosion-corrosion [46]. During electrolysis, the cathode is protected against corrosion;  
376 however, under stop conditions, it is vulnerable to corrosion [47]. The dual-layered anode and  
377 subsequent activation can improve the resistance against chloride-induced pitting corrosion  
378 [38].

379

380

381

#### 382           **5.4. Degradation of electrocatalysts**

383           Metallic substrates such as Ti passivate through the growth of an insulating oxide layer.  
384           An intermediate layer of IrO<sub>2</sub> or Sn-doped IrO<sub>2</sub> on Ti substrates primarily prevents the oxide  
385           growth on the substrate [33]. With the intimate contact between substrate and catalyst, not only  
386           *R*<sub>ct</sub> decreases but also the durability improves; thus, Ni-based structures grown directly from a  
387           nickel foam are preferred in the design of integrated catalysts [19].

388           Ledendecker *et al.* [47] studied the stability and corrosion of several PGM-free cathodes,  
389           including metal carbides (WC), sulfides (MoS<sub>2</sub>), phosphides (Ni<sub>5</sub>P<sub>4</sub>, Co<sub>2</sub>P), their base metals  
390           (W, Ni, Mo, Co), as well as Pt in an acidic medium. Under zero current density, the dissolution  
391           of phosphides, carbides and sulfides was drastically reduced compared to their base metal  
392           samples. Under operation, their dissolution rate was similar to the pure metals. Successive start-  
393           stop cycles and the electrode/electrolyte contact before electrolysis resulted in more severe  
394           corrosion. They proposed that the pretreatment of the catalyst can remove dangling bonds,  
395           defects and surface oxides and increase the durability of the electrodes.

396           Claudel *et al.* [48] reported that nanostructured IrO<sub>x</sub> anodes change during OER process.  
397           They verified several morphological changes like migration, agglomeration, coalesce and  
398           detaching. Gradual oxidation of Ir(0) and Ir(III) to Ir(IV) and Ir(V) and enhanced local  
399           accumulation of hydroxyl/water species on IrO<sub>x</sub> nanocatalysts were the main influencing  
400           factors. In contrast, for the micro-sized IrO<sub>x</sub> anodes, no water/hydroxyl coverage was observed  
401           [48].

402           Accelerated degradation tests for thin SrIrO<sub>3</sub> films showed that anodic OER potentials  
403           result in the partial dissolution of the flat surface of SrIrO<sub>3</sub> to a rough IrO<sub>x</sub>-rich one. The IrO<sub>3</sub>  
404           dissolution rate is potential-dependent and Sr dissolves with a stoichiometric rate, resulting in  
405           an IrO<sub>x</sub>-rich layer. Despite this, their bulk remains in its original perovskite structure [49].

406 For Co<sub>2</sub>P HER electrocatalysts, Zhang *et al.* [50] indicated that the dissolution mechanism  
407 was strongly dependent upon the pH; in acidic solution, the components dissolved  
408 stoichiometrically but in alkaline pH, the degradation proceeded through hydroxide formation  
409 with preferential dissolution of P over Co.

410

## 411 **6. Techno-economic insights**

412 Regardless of developments in non-PGM electrocatalysts, practical applications require a  
413 pretreatment (such as reverse osmosis or alkali treatment) that imposes high costs equal to  
414 those of currently used PGM-based fresh-water electrolyzers. Commercial PEMWEs currently  
415 use PGM-based electrodes; however, the emerging AEMWEs are promising candidates for  
416 future applications, because they can operate with low-cost electrocatalysts. Generally, for H<sub>2</sub>  
417 production, two economic insights can be suggested [51]:

418 (a) A one-step strategy in which seawater is directly used without any pretreatment, the  
419 research is then focused on the design of low-cost, selective and stable materials.

420 (b) A two-step path that uses desalination plants (mostly reverse osmosis). With this  
421 strategy, the research efforts and costs are focused on the decrease of desalination costs.

422 Recently, Farràs *et al.* [51] revealed that from an energy and economic point-of-view, the  
423 two-step strategy is currently more practical. However, regarding the emerging technologies  
424 that are introduced in developing low-cost, stable electrocatalysts and new cell configurations,  
425 energy/economic analysis and revisiting the strategies must be regularly performed.

426

## 427 **7. Closing remarks**

428 Seawater is potentially an infinite resource for hydrogen (and oxygen) production, but  
429 complicated composition is a big challenge for its direct electrolysis. The most promising non-  
430 PGM cathodic catalysts are based upon transition metal oxides, carbides, chalcogenides, and

431 especially phosphides and nitrides. TMPs and TMNs with high intrinsic conductivity and  
432 corrosion resistances are highly efficiency and stable in seawater; thus, they can be considered  
433 as the most promising non-PGM materials for HER. Negatively charged surface sites trigger  
434 the H-adsorption, while positively charged sites prefer interaction with hydroxide and weaken  
435 H-OH bonds in water molecules. Doping electronegative/electron-withdrawing species  
436 facilitates the formation of these separated adsorption sites and promotes HER. For OER,  
437 highly selective Ni-Fe LDH based catalysts are the most promising non-PGM anodes as  
438 candidates for future commercialization purposes.

439 Generally, for both HER and OER electrodes, a holey nanostructure and high  
440 conductivity of electrocatalysts are vital for enhancing the electrode efficiency. Intimate  
441 contact between catalyst and substrate, and integrated electrodes results in facilitated charge  
442 transfer with increased stability. The use of carbonaceous nanomaterials can also provide an  
443 electron transfer path between catalyst components.

444 Ni-Fe LDH anodes have been used in a model AEMWE and showed their potential for future  
445 applications. However, even the best-studied catalysts have not shown stabilities over 1,000h  
446 of electrolysis at current densities not much higher than  $200\text{mA}/\text{cm}^2$ ; while future seawater  
447 electrolysers must work with current densities of at least  $1\text{A}/\text{cm}^2$  to fulfill the economic  
448 expectations.

449 Another unsolved challenge is the need for seawater purification before electrolysis. The use  
450 of an asymmetric feed with direct seawater in the cathode and circulating KOH in anode  
451 compartments, or the use of the NaCl salting-out effect in highly concentrated NaOH have  
452 been reported; however, there is an urgent need for developing the studies in this regard.

453

454 **Conflict of interest statement**

455 Nothing declared.

456 **Acknowledgement**

457 The authors would like to thank the ENERSENSE programme.

458

Journal Pre-proof



459 **References**

460 Papers of particular interest, published within the period of review, have been highlighted as:

461 \*of special interest

462 \*\*of outstanding interest

463 [1] B.G. Pollet, J.J. Lamb, eds., Hydrogen, Biomass and Bioenergy - 1st Edition Integration  
464 Pathways for Renewable Energy Applications, 1st ed., Academic Press, 2020.

465 [https://ec.europa.eu/energy/sites/ener/files/hydrogen\\_strategy.pdf](https://ec.europa.eu/energy/sites/ener/files/hydrogen_strategy.pdf) (Accessed:  
466 19.10.2021).

467 [2] A Wood Mackenzie Business.

468 [https://www.greentechmedia.com/articles/read/us-firm-unveils-worlds-largest-green-](https://www.greentechmedia.com/articles/read/us-firm-unveils-worlds-largest-green-hydrogen-project)  
469 [hydrogen-project](https://www.greentechmedia.com/articles/read/us-firm-unveils-worlds-largest-green-hydrogen-project) (2020) (Accessed: 19.10.2021).

470 [3] Z. Liu, B. Han, Z. Lu , W. Guan, Y. Li , C. Song , L. Chen, S C. Singhal, Efficiency  
471 and stability of hydrogen production from seawater using solid oxide electrolysis cells,  
472 Appl. Energy, 300 (2021) 117439. <https://doi.org/10.1016/j.apenergy.2021.117439>.

473 [4] R. d'Amore-domenech, O. Santiago, T.J. Leo, Multicriteria analysis of seawater  
474 electrolysis technologies for green hydrogen production at sea, 133 (2020) 110166  
475 <https://doi.org/10.1016/j.rser.2020.110166>.

476 [5] S. Dresp, F. Dionigi, M. Klingenhof, P. Strasser, Direct Electrolytic Splitting of  
477 Seawater: Opportunities and Challenges, ACS Energy Letters, 4 (2019) 933–942.  
478 <https://doi.org/10.1021/acsenergylett.9b00220>

479 [6] \*W. Tong, M. Forster, F. Dionigi, S. Dresp, R.S. Erami, P. Strasser, A.J. Cowan, P.  
480 Farràs, Electrolysis of low-grade and saline surface water, Nat. Energy 5 (2020) 367–  
481 377. <https://doi.org/10.1038/s41560-020-0550-8>.

482 \*These authors provided a comprehensive review on recent developments in electrode  
483 materials/catalysts for water electrolysis using low-grade and saline water. They  
484 presented challenges of electrolyzers and future potential strategies for having highly  
485 active/selective electrocatalysts. The effects of the presence of seawater impurities such  
486 as cations, chloride and bio-organisms have also been mentioned in this paper.

487 [7] J. Fauvarque, The chlorine industry. *Pure. Appl. Chem.* 68 (1996) 1713–1720.  
488 <https://doi.org/10.1351/pac199668091713>

489 [8] I. Moussallem, J. Jörissen, U. Kunz, S. Pinnow, and T. Turek, Chlor-alkali electrolysis  
490 with oxygen depolarized cathodes: history, present status and future prospects, *J. App.*  
491 *Electrochem.* 38 (2008) 1177-1194. <https://doi.org/10.1007/s10800-008-9556-9>

492 [9] Y. Zhao, Q. Tang, B. He, P. Yang, Carbide decorated carbon nanotube electrocatalyst  
493 for high-efficiency hydrogen evolution from seawater, *RSC Adv.* 6 (2016) 93267–  
494 93274. <https://doi.org/10.1039/C6RA17839A>

495 [10] G. Zhou, Z. Guo, Y. Shan, S. Wu, High-efficiency hydrogen evolution from  
496 seawater using hetero-structured T/Td phase ReS<sub>2</sub> nanosheets with cationic vacancies,  
497 *Nano Energy* 55 (2019) 42–48. <https://doi.org/10.1016/j.nanoen.2018.10.047>.

498 [11] \*M. Sarno, E. Ponticorvo, D. Scarpa, Active and stable graphene  
499 supporting trimetallic alloy-based electrocatalyst for hydrogen evolution by  
500 seawater splitting, *Electrochem. Commun.* 111 (2020) 106647.  
501 <https://doi.org/10.1016/j.elecom.2019.106647>.

502 \*This paper introduces non-noble metal electrocatalysts containing Ni, Ru and  
503 graphene towards HER in seawater, exhibiting 200h stable performance and almost  
504 100% H<sub>2</sub> production efficiency. The synergistic alloying effects were shown that had a  
505 significant role on their improved performances. The use of graphene support was also

506 mentioned as another reason of their behavior. The highly active Ir and the stability of  
507 Ir and Ru, competitive dissolution rates of different components were also other reasons  
508 of their corrosion resistances.

509 [12] A. Lam, H. Li, S. Zhang, H. Wang, D.P. Wilkinson, S. Wessel, and T.T. Cheng, Ex-  
510 situ study of chloride contamination on carbon supported Pt catalyst, *J. Power Sources*,  
511 205 (2012) 235-238. <https://doi.org/10.1016/j.jpowsour.2012.01.063>

512 [13] S. Geiger, S. Cherevko, and K.J. Mayrhofer, Dissolution of platinum in presence of  
513 chloride traces, *Electrochim. Acta* 179 (2015) 24-31.  
514 <https://doi.org/10.1016/j.electacta.2015.03.059>

515 [14] L. Xiu, W. Pei, S. Zhou, Z. Wang, P. Yang, J. Zhao, J. Qiu, Multilevel Hollow MXene  
516 Tailored Low-Pt Catalyst for Efficient Hydrogen Evolution in Full-pH Range and  
517 Seawater, *Adv. Functional Mater.* 30 (2020) 1910028;  
518 <https://doi.org/10.1002/adfm.201910028>

519 [15] F. Yu, L. Yu, I.K. Mishra, Y. Yu, Z.F. Ren, H.Q. Zhou, Recent developments in earth-  
520 abundant and non-noble electrocatalysts for water electrolysis, *Mater. Today Phys.* 7  
521 (2018) 121-138. <https://doi.org/10.1016/j.mtphys.2018.11.007>

522 [16] X. Niu, Q. Tang, B. He, P. Yang, Robust and stable ruthenium alloy electrocatalysts  
523 for hydrogen evolution by seawater splitting, *Electrochim. Acta.* 208 (2016) 180–187.  
524 <https://doi.org/10.1016/j.electacta.2016.04.184>

525 [17] B. Debnath, S. Parvin, H. Dixit, and S. Bhattacharyya, Oxygen- Defect Rich  
526 Cobalt Ferrite Nanoparticles for Practical Water Electrolysis with Sublime  
527 Activity and Durability, *Chem. Sus. Chem.* 13 (2020), 3875-3886.  
528 <https://doi.org/10.1002/cssc.202000932>

- 529 [18] X. Lu, J. Pan, E. Lovell, T.H. Tan, Y.H. Ng, R. Amal, A sea-change: Manganese  
530 doped nickel/nickel oxide electrocatalysts for hydrogen generation from seawater,  
531 Energy Environ. Sci. 11 (2018) 1898-1910. <https://doi.org/10.1039/C8EE00976G>
- 532 [19] \*\*X. Gao, Y. Chen, T. Sun, J. Huang, W. Zhang, Q. Wang, R. Cao, Karst landform-  
533 featured monolithic electrode for water electrolysis in neutral media, Energy Environ.  
534 Sci. 13 (2020) 174-182. <https://doi.org/10.1039/c9ee02380a>
- 535 \*\*Nickel foam-based, high performance, bi-functional electrocatalysts were formed  
536 with Ni sites on valleys and nickel oxide sites on towers. The authors showed that the  
537 electrode had an easy switching ability between HER and OER catalysis. The paper  
538 presents careful discussion about the effects of structure on performance.
- 539 [20] Q. Lv, J. Han, X. Tan, W. Wang, L. Cao, B. Dong, Feather-like NiCoP holey  
540 nanoarrays for efficient and stable seawater splitting, ACS Appl. Energy Mater. 2  
541 (2019) 3910–3917. <https://doi.org/10.1021/acsaem.9b00599>.
- 542 [21] Y. Ma, C. Wu, X. Feng, H. Tan, L. Yan, Highly efficient hydrogen evolution from  
543 seawater by a low-cost and stable CoMoP@C electrocatalyst superior to Pt/C, Energy  
544 Environment Sci. 10 (2017) 788–798. <https://doi.org/10.1039/c6ee03768b>
- 545 [22] D.V. Esposito, S.T. Hunt, Y.C. Kimmel, J.G. Chen, A New Class of Electrocatalysts  
546 for Hydrogen Production from Water Electrolysis: Metal Monolayers Supported on  
547 Low-Cost Transition Metal Carbides, J. Am. Chem. Soc. 134 (2012) 3025–3033.  
548 <https://doi.org/10.1021/ja208656v>
- 549 [23] L. Wu, L. Yu, F. Zhang, B. McElhenny, D. Luo, A. Karim, S. Chen, and Z. Ren,  
550 Heterogeneous Bimetallic Phosphide Ni<sub>2</sub>P-Fe<sub>2</sub>P as an Efficient Bifunctional Catalyst  
551 for Water/Seawater Splitting, Adv. Funct. Mater. 31 (2020) 2006484.  
552 <https://doi.org/10.1002/adfm.202006484>

- 553 [24] H. Jin, X. Liu, A. Vasile, Y. Jiao, Y. Zhao, Y. Zheng, S. Qiao, Single-Crystal  
554 Nitrogen-Rich Two-Dimensional Mo<sub>5</sub>N<sub>6</sub> Nanosheets for Efficient and Stable Seawater  
555 Splitting, ACS Nano. 12 (2018) 12761–12769.  
556 <https://doi.org/10.1021/acsnano.8b07841>
- 557 [25] B. Sebek, S. Butkut, I. Savickaja, M. Petrulevi, A. Selskis, R. Ramanauskas, V.  
558 Jasulaitien, Electrolytic splitting of saline water: Durable nickel oxide anode for  
559 selective oxygen evolution, Int. J. Hydrogen Energy. 4 (2019) 5929–5939.  
560 <https://doi.org/10.1016/j.ijhydene.2019.01.120>
- 561 [26] \*\*B. Cui, Z. Hu, C. Liu, S. Liu, F. Chen, S. Hu, J. Zhang, W. Zhou, Y. Deng, Z. Qin,  
562 Z. Wu, Y. Chen, L. Cui, W. Hu, Heterogeneous lamellar-edged Fe-Ni(OH)<sub>2</sub>/Ni<sub>3</sub>S<sub>2</sub>  
563 nanoarray for efficient and stable seawater oxidation, Nano Res. 14 (2021) 1149–1155.  
564 <https://doi.org/10.1007/s12274-020-3164-3>
- 565 \*\*In this paper, the authors reported a Ni<sub>3</sub>S<sub>2</sub> nanoarray with Fe-Ni(OH)<sub>2</sub> lamellar edges  
566 and significantly enhanced amount of adsorption sites; they were very efficient towards  
567 the OER. The morphology and 3D lamellar-edged structure had special effects on the  
568 electrode performance. OER efficiency of almost 95% with Fe sites that presented  
569 selectivity over OER were the main features of these electrodes.
- 570 [27] S. Gupta, M. Forster, A. Yadav, A.J. Cowan, N. Patel, M. Patel, Highly Efficient  
571 and Selective Metal Oxy-Boride Electrocatalysts for Oxygen Evolution from Alkali  
572 and Saline Solutions, ACS Appl. Energy Mater. 3 (2020) 7619–7628.  
573 <https://doi.org/10.1021/acsaem.0c01040>
- 574 [28] T.P. Keane, D.G. Nocera, Selective Production of Oxygen from Seawater by Oxidic  
575 Metallate Catalysts, ACS Omega. 4 (2019) 12860–12864.  
576 <https://doi.org/10.1021/acsomega.9b01751>

- 577 [29] W.H. Hung, B.Y. Xue, T.M. Lin, S.Y. Lu, I-Yu Tsao, A Highly Active Selenized  
578 Nickel-Iron Electrode with Layered Double Hydroxide for Electrocatalytic Water  
579 Splitting in Saline Electrolyte, *Materials Today Energy*, 19 (2021) 100575.  
580 <https://doi.org/10.1016/j.mtener.2020.100575>
- 581 [30] L. Yu, Q. Zhu, S. Song, B. Mcelhenny, D. Wang, C. Wu, Z. Qin, J. Bao, Y. Yu, S.  
582 Chen, Z. Ren, Non-noble metal-nitride based electrocatalysts for high-performance  
583 alkaline seawater electrolysis, *Nat. Commun.* 10 (2019) 5106.  
584 <https://doi.org/10.1038/s41467-019-13092-7>
- 585 [31] Y. Zhao, B. Jin, Y. Zheng, H. Jin, Y. Jiao, S. Qiao, Charge State Manipulation of  
586 Cobalt Selenide Catalyst for Overall Seawater Electrolysis, *Adv. Energy Mater.* 8  
587 (2018) 1801926. <https://doi.org/10.1002/aenm.201801926>
- 588 [32] J.S. Ko, J.K. Johnson, P.I. Johnson, Z. Xia, Decoupling Oxygen and Chlorine  
589 Evolution Reactions in Seawater using Iridium-based Electrocatalysts, *Chem.Cat.*  
590 *Chem.* 12 (2020) 4526-4532. <https://doi.org/10.1002/cctc.202000653>
- 591 [33] J.G. Vos, T.A. Wezendonk, A.W. Jeremiasse, M.T.M. Koper, MnO<sub>x</sub>/IrO<sub>x</sub> as Selective  
592 Oxygen Evolution Electrocatalyst in Acidic Chloride Solution, *J. Am. Chem. Soc.* 140  
593 (2018) 10270–10281. <https://doi.org/10.1021/jacs.8b05382>
- 594 [34] L. Bigiani, D. Barreca, A. Gasparotto, T. Andreu, J. Verbeeck, C. Sada, E. Modin,  
595 O.I. Lebedev, J.R. Morante, C. Maccato, Selective anodes for seawater splitting via  
596 functionalization of manganese oxides by a plasma-assisted process, *Appl. Catal. B*  
597 *Environ.* 284 (2021) 119684. <https://doi.org/10.1016/j.apcatb.2020.119684>
- 598 [35] F. Dionigi, T. Reier, Z. Pawolek, M. Gliuch and P. Strasser, Design Criteria, Operating  
599 Conditions, and Nickel–Iron Hydroxide Catalyst Materials for Selective Seawater

600 Electrolysis, Chem. Sus. Chem. 9 (2016) 962–972.  
601 <https://doi.org/10.1002/cssc.201501581>

602 [36] \*\*S. Dresp, T.N. Thanh, M. Klingenhof, S. Brückner, P. Hauke and P. Strasser,  
603 Efficient direct seawater electrolyzers using selective alkaline NiFe-LDH as OER  
604 catalyst in asymmetric electrolyte feeds, Energy Environ. Sci., 13 (2020) 1725-1729.  
605 <https://doi.org/10.1039/d0ee01125h>

606 \*\* A promising seawater electrolyser configuration was proposed by authors in this paper.  
607 They used an asymmetric electrolyte feed strategy. The electrolytes based on seawater and  
608 KOH were used in different cell compartments with a NiFe-LDH based anode as a potential  
609 anode material for future non-precious metal electrodes. A significant selectivity was  
610 obtained with this type of anode even at cell potentials beyond 3.0 V(cell voltage). They  
611 showed that direct feed of neutral seawater at the cathode in a single pass and circulating  
612 pure KOH electrolyte at the anode yielded the best performance of the cells.

613 [37] J. Lu, C. Li, H. Wang, S. Ji, X.Wang, R. Wang, How to get to best oxygen evolution  
614 behavior from the electrolysis practice of the seawater, Int. J. Hydrogen Energy, 46  
615 (2021) 12936-12943. <https://doi.org/10.1016/J.IJHYDENE.2021.01.139>

616 [38] J. Mohammed-Ibrahim, H. Moussab, Recent advances on hydrogen production  
617 through seawater electrolysis, Mater. Sci. Energy Tech. 3 (2020) 780-807.  
618 <https://doi.org/10.1016/j.mset.2020.09.005>

619 [39] S. Dresp, F. Luo, R. Schmack, S. Kühl, M. Gliech, P. Strasser, An efficient  
620 bifunctional two-component catalyst for Oxygen Reduction and Oxygen Evolution in  
621 reversible fuel cells, electrolyzers and rechargeable air electrodes, Energy Environ.  
622 Sci., 9 (2016) 2020-2024. <https://doi.org/10.1039/C6EE01046F>

- 623 [40] S. Dresp, F. Dionigi, S. Loos, J. Ferreira de Araujo, C. Spöri, M. Gliech, H. Dau,  
624 P. Strasser, Direct Electrolytic Splitting of Seawater: Activity, Selectivity, Degradation,  
625 and Recovery Studied from the Molecular Catalyst Structure to the Electrolyzer Cell  
626 Level, *Adv. Energy Mater.* 8 (2018) 1800338.  
627 <https://doi.org/10.1002/aenm.201800338>
- 628 [41] \*\*S. Dresp, F. Dionigi, M. Klingenhof, T. Merzdorf, H. Schmies, J. Drnec, A.  
629 Poulain, and P. Strasser, Molecular Understanding of the Impact of Saline  
630 Contaminants and Alkaline pH on NiFe Layered Double Hydroxide Oxygen Evolution  
631 Catalysts, *ACS Catal.* 11 (2021) 6800–6809; <https://doi.org/10.1021/acscatal.1c00773>  
632 \*\* The authors investigated the structural transformations of NiFe LDH, as the state-  
633 of-the-art anode catalyst for direct seawater electrolyzers, with different chloride  
634 concentrations and pH values. They analyzed the  $\alpha \leftrightarrow \gamma$  phase's transformations and the  
635 effect of salt concentration on them that affected the catalytic activity of the electrodes.
- 636 [42] G. Amikam, P. Nativ, Y. Gende, Chlorine-free alkaline seawater electrolysis for  
637 hydrogen production, *Int. J. Hydrogen Energy*, 43 (2018) 6504-6514.  
638 <https://doi.org/10.1016/j.ijhydene.2018.02.082>
- 639 [43] R. Balaji, B. Suresh, J. Lakshmi, N. Senthil, An alternative approach to selective sea  
640 water oxidation for hydrogen production, *Electrochem. Commun.* 11 (2009) 1700–  
641 1702. <https://doi.org/10.1016/j.elecom.2009.06.022>
- 642 [44] S. Khatun, H. Hirani, and P. Roy, Seawater electrocatalysis: activity and selectivity.  
643 *J. Mater. Chem. A* 9 (2021) 74-86. <https://doi.org/10.1039/D0TA08709B>
- 644 [45] F. Cheng, X. Feng, X. Chen, W. Lin, J. Rong, W. Yang, Synergistic action of Co-Fe  
645 layered double hydroxide electrocatalyst and multiple ions of sea salt for efficient



- 646 seawater oxidation at near-neutral pH, *Electrochim. Acta.* 251 (2017) 336–343.  
647 <https://doi.org/10.1016/j.electacta.2017.08.098>
- 648 [46] T. Hodgkiess, G. Vassiliou, Complexities in the erosion corrosion of copper-nickel  
649 alloys in saline water, *Desalination* 183 (2005) 235-247.  
650 <https://doi.org/10.1016/j.desal.2005.03.037>
- 651 [47] M. Ledendecker, J.S. Mondschein, O. Kasian, S. Geiger, D. Göhl, M. Schalenbach,  
652 A. Zeradjanin, S. Cherevko, R.E. Schaak, K. Mayrhofer, Stability and activity of non-  
653 noble based catalysts toward the hydrogen evolution reaction – feasible electrocatalysts  
654 in acidic medium?, *Angewandte Chemie.* 56 (2017) 9767-9771. [https://doi.org/](https://doi.org/10.1002/anie.201704021)  
655 [10.1002/anie.201704021](https://doi.org/10.1002/anie.201704021)
- 656 [48] F. Claudel, L. Dubau, G.y Berthomé, L.Sola-Hernandez, C. Beauger, L. Piccolo, F.  
657 Maillard Degradation Mechanisms of Oxygen Evolution Reaction Electrocatalysts: A  
658 Combined Identical-Location Transmission Electron Microscopy and X-ray  
659 Photoelectron Spectroscopy Study, *ACS Catal.* 9 (2019) 4688–4698.  
660 <https://doi.org/10.1021/acscatal.9b00280>
- 661 [49] M. Ben-Naim, Y. Liu, M. B. Stevens, K. Lee, M. R. Wette, A. Boubnov, A. A.  
662 Trofimov, A. V. Ievlev, A. Belianinov, R. C. Davis, B. M. Clemens, S. R. Bare, Y.  
663 Hikita, H.Y. Hwang, D.C. Higgins, R. Sinclair, and T. F. Jaramillo, Understanding  
664 Degradation Mechanisms in SrIrO<sub>3</sub> Oxygen Evolution Electrocatalysts: Chemical and  
665 Structural Microscopy at the Nanoscale, *Adv. Funct. Mater.* 31 (2021) 2101542,  
666 <https://doi.org/10.1002/adfm.202101542>
- 667 [50] Y. Zhang, L. Gao, E.J. M. Hensen, and J. P. Hofmann, Evaluating the Stability of  
668 Co<sub>2</sub>P Electrocatalysts in the Hydrogen Evolution Reaction for Both Acidic and

669 Alkaline Electrolytes, ACS Energy Lett. 3 (2018) 1360–1365.

670 <https://doi.org/10.1021/acsenergylett.8b00514>

671 [51] P. Farràs, P. Strasser, A.J. Cowan, Previews Water electrolysis: Direct from the sea

672 or not to be? Joule 5 (2021) 1921-1923. <https://doi.org/10.1016/j.joule.2021.07.014>

673

Journal Pre-proof

**Declaration of interests**

The authors declare that they have no known competing financial interests or personal relationships that could have appeared to influence the work reported in this paper.

The authors declare the following financial interests/personal relationships which may be considered as potential competing interests:

Journal Pre-proof